


Dual bulk-boundary correspondence in a nonreciprocal spin-orbit coupled zigzag latticeLingfang Li,¹ Chong Hou,¹ Gangzhou Wu,¹ Yang Ruan,¹ Shihua Chen^{1,2,*}, Luqi Yuan^{3,†} and Zhenhua Ni^{1,2,‡}¹*School of Physics and Frontiers Science Center for Mobile Information Communication and Security, Southeast University, Nanjing 211189, China*²*Purple Mountain Laboratories, Nanjing 211111, China*³*State Key Laboratory of Advanced Optical Communication Systems and Networks, School of Physics and Astronomy, Shanghai Jiao Tong University, Shanghai 200240, China* (Received 12 November 2023; revised 21 March 2024; accepted 18 June 2024; published 1 July 2024)

We unveil a relevant non-Hermitian symmetry and hence a dual bulk-boundary correspondence (BBC) from a one-dimensional non-Hermitian Rice-Mele model including on-site dissipation, nonreciprocity, and spin-orbit coupling. To expose this dual BBC, we present the closed-form solutions for spin-up and spin-down edge modes and two explicit topological winding numbers, which are linked to each other to a perfect degree. We also demonstrate the topological zero modes and their strong insensitivity to disorder in the presence of spin-orbit coupling. We anticipate that this dual BBC may offer another route for manipulating spin currents and trigger the research for dual topological insulators in a single zigzag lattice.

DOI: [10.1103/PhysRevB.110.L041103](https://doi.org/10.1103/PhysRevB.110.L041103)

As a central figure in topological band theory [1–3], the bulk-boundary correspondence (BBC) has attracted significant attention in diverse areas such as condensed state physics [4,5], mechanics [6], electronics [7], acoustics [8], plasma physics [9], and photonics [10,11]. It depicts that the existence of gapless boundary states that are insensitive to defects and disorder [12] can be related to the topological invariants of the bulk, a global geometric property of Bloch wave functions calculated in momentum space [10]. Such BBC principle prevails in Hermitian systems for predicting the topological phases of matter [13], leading to the discovery of numerous topological insulators [14,15]. Meanwhile, the duality behind the BBC has also sparked off new ideas for other subjects, e.g., proposing the modulation instability-rogue wave correspondence for predicting rare extreme waves in nonlinear systems [16].

Nonetheless, when the Hamiltonian inherently exhibits non-Hermiticity [17–21], the spectra and eigenstates of the bulk can be drastically changed under an open boundary condition (OBC), owing to the presence of a non-Hermitian skin effect [22–27]. As a consequence, the topological invariants obtained still with a Bloch Hamiltonian may no longer predict the boundary states, foreshadowing the breakdown of the conventional BBC [28,29]. One way to overcome this difficulty is to define a real-space invariant, based on the notion of biorthogonal quantum mechanics, hence called biorthogonal BBC [30,31]. Another more straightforward way is to utilize the concept of generalized Brillouin zone (GBZ) [22,32–34], which can allow the topological invariants to be correctly defined in momentum space, resulting in a so-called non-Bloch BBC [35–38]. To date, both non-Bloch BBC and

non-Hermitian skin effects have been experimentally confirmed in such physical settings as electric circuits [39], mechanical metamaterials [40], photonic lattices [41,42], and quantum walks [43].

In developing the formalism of BBC, the role of symmetry of non-Hermitian systems cannot be overemphasized [13,18,44,45]. It has recently been demonstrated that non-Hermiticity expands significantly the celebrated Altland-Zirnbauer symmetry classification [46] and a total of 38 symmetry classes are identified, whereby different topological invariants can be defined [47]. In this Letter, we unveil an interesting symmetry that is not included in that classification, but proper to the one-dimensional (1D) non-Hermitian Rice-Mele (RM) model [48], which, when combining the on-site gain and loss [49–52], nonreciprocity [33,53], and spin-orbit (SO) coupling [54–56], does not respect any known internal symmetries, e.g., chiral symmetry (CS). In non-Hermitian systems, this symmetry is actually universal, despite receiving little attention in the past. What we report here is that it entails two topological invariants that underpin the topological edge states in such antichiral RM model. Our results conform to the recent experimental observation that the 1D zigzag photonic lattices with broken CS do admit quantized Zak phase [57].

Furthermore, we obtain the closed-form, asymptotically exact analytic solutions for topological edge modes, along with their parameter conditions. A so-called dual BBC is established, by which we mean that the two topological winding numbers can precisely predict whether or not the topological edge modes are available for spin-up electrons and spin-down ones, respectively. This concept can be reminiscent of the stacked dual topology found in 3D superlattices [58–60], despite having an entirely different origin. It is anticipated that, when the values of both topological invariants become nonzero, a dual topological insulator phase would appear in

*Contact author: cshua@seu.edu.cn†Contact author: yuanluqi@sjtu.edu.cn‡Contact author: zhni@seu.edu.cn

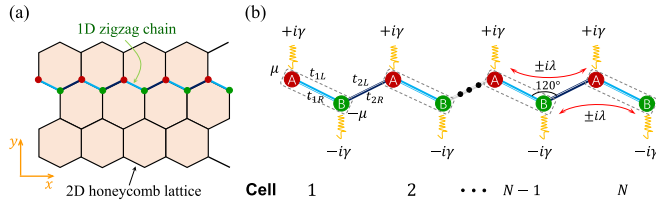


FIG. 1. (a) A schematic sketch of a 2D transversely periodic honeycomb lattice that can be seen as a stack of 1D zigzag chains. (b) Geometry of an open 1D tight-binding zigzag model of N cells, with $t_{1L,R}$ (sky-blue lines) and $t_{2L,R}$ (dark-blue lines) being nonreciprocal hopping amplitudes.

a 1D zigzag chain. These results fully uncover the mystery behind the BBC, with which one can even predict the topological edge modes without the knowledge of the topology of non-Hermitian systems [61–63].

For our studies, we consider the following Hamiltonian of the generalized 1D non-Hermitian RM model [48]

$$\hat{H} = \sum_{n=1}^N [t_{1L}\hat{a}_n^\dagger\hat{b}_n + t_{1R}\hat{b}_n^\dagger\hat{a}_n + (i\gamma + \mu)(\hat{a}_n^\dagger\hat{a}_n - \hat{b}_n^\dagger\hat{b}_n)] + \sum_{n=1}^{N-1} (t_{2R}\hat{a}_{n+1}^\dagger\hat{b}_n + t_{2L}\hat{b}_{n+1}^\dagger\hat{a}_n) + \sum_{n=1}^{N-1} (-i\lambda\hat{a}_n^\dagger\sigma_z\hat{a}_{n+1} + i\lambda\hat{b}_n^\dagger\sigma_z\hat{b}_{n+1} + \text{H.c.}), \quad (1)$$

where $\hat{a}_n^\dagger = (\hat{a}_{n\uparrow}^\dagger, \hat{a}_{n\downarrow}^\dagger)$ and $\hat{b}_n^\dagger = (\hat{b}_{n\uparrow}^\dagger, \hat{b}_{n\downarrow}^\dagger)$ stand for the creation operators on the sublattice A and B of the n th unit cell, respectively, for electrons with spin up (\uparrow) or spin down (\downarrow), σ_z is the Pauli matrix, and H.c. denotes the Hermitian conjugate. This tight-binding Hamiltonian is the 1D version of the Kane-Mele model [54,55] used in graphene [64] and silicene [65] for unveiling the quantum spin Hall effect. It thus corresponds to the 1D zigzag chain geometry spanning across the bulk of a 2D honeycomb lattice [see Fig. 1(a)] [66–68], obtained by Fourier transforming the latter along the translationally invariant y direction [69]. Here, N is the cell number of the lattice, $\mu \in \mathbb{R}$ is the staggered sublattice potential, $\gamma \in \mathbb{R}$ is the on-site gain and loss, $\lambda \in \mathbb{R}$ is the SO coupling, and $t_{1L,R}$ ($t_{2L,R}$) represent the nonreciprocal intracell (intercell) hopping amplitudes [see Fig. 1(b)]. For analytical purposes, we do not include the Rashba SO coupling effect [70], which could render electronic spins inseparable. Actually, in that case, our analytical solutions provided here would still work fairly well for predicting topological edge states, as long as the Rashba SO coupling is comparatively weak [71,72] (see Sec. VII in Supplemental Material [73]).

Performing a Fourier transformation on Eq. (1), one can obtain the generalized Bloch Hamiltonian $\mathcal{H}(\beta \equiv e^{ik})$ as

$$\mathcal{H}(\beta) = \begin{bmatrix} \mathcal{H}_\uparrow(\lambda, \beta) & \mathbf{0} \\ \mathbf{0} & \mathcal{H}_\downarrow(\lambda, \beta) \end{bmatrix}_{4 \times 4}, \quad (2)$$

where $\mathcal{H}_\uparrow(\lambda, \beta)$ and $\mathcal{H}_\downarrow(\lambda, \beta)$ are the traceless spin-up and spin-down Bloch Hamiltonians, defined by

$$\mathcal{H}_\uparrow(\lambda, \beta) = \begin{bmatrix} G(\lambda, \beta) & R_+(\beta) \\ R_-(\beta) & -G(\lambda, \beta) \end{bmatrix},$$

$$\mathcal{H}_\downarrow(\lambda, \beta) = \mathcal{H}_\uparrow(-\lambda, \beta), \quad (3)$$

with $R_+(\beta) = t_{1L} + t_{2R}/\beta$, $R_-(\beta) = t_{1R} + t_{2L}\beta$, and $G(\lambda, \beta) = \mu + i\gamma + i\lambda(\beta^{-1} - \beta)$. This momentum-space Hamiltonian (2) gives the entire spectrum $E = \{E_\uparrow\} \cup \{E_\downarrow\}$, where E_\uparrow and E_\downarrow are the eigenenergies of spin-up and spin-down electronic states, determined by

$$R_+(\beta)R_-(\beta) + G(\lambda_\sigma, \beta)^2 = E_\sigma^2. \quad (4)$$

Here, we use σ to indicate the spin up (\uparrow) or spin down (\downarrow), and let $\lambda_\sigma = \lambda$ or $-\lambda$ as σ takes \uparrow or \downarrow . It should be noted that under the periodic boundary condition (PBC), the energy spectrum E can be solely determined by Eq. (4), with $\beta = e^{ik}$ and letting k run from 0 to 2π .

As one can check, the generalized RM Hamiltonian respects neither the sublattice symmetry (SLS) nor the CS [57,78], let alone the \mathcal{PT} or anti- \mathcal{PT} symmetry [51,79] (see also Supplemental Material [73] for details). However, the Hamiltonian could respect $\mathcal{S}\mathcal{H}^\dagger(k)\mathcal{S}^{-1} = -\mathcal{H}(k)$ (seen in momentum space), where \mathcal{S} is a unitary matrix satisfying $\mathcal{S}\mathcal{S}^* = -\mathbb{1}$ and T means transpose. This latter symmetry implies that, if $|u(k)\rangle$ is the right eigenstate of $\mathcal{H}(k)$ with eigenenergy $E(k)$, then $\mathcal{S}|u^*(k)\rangle$ is the left eigenstate of $\mathcal{H}(k)$ with $-E(k)$ [47]. This represents a physically relevant symmetry and basically it can be realized by a combined action of a parity operator and a particle-hole operator. Moreover, one can prove that it is also relevant for defining the topological invariant with line gap [73]. In many non-Hermitian systems where SLS fails [80,81], this symmetry still works to ensure the stable transport of topological edge states. For this reason, we will term it SLS † to distinguish it from conventional SLS.

Owing to the SLS † , the eigenvalue equation $\hat{H}|\psi\rangle = E|\psi\rangle$ of the Hamiltonian (1) under OBC can be exactly solved in real space, for both the energy spectrum E and the eigenstates $|\psi\rangle$ [73]. Here, we only present the asymptotic analytic solutions for topological edge states, along with the parameter conditions for their existence. Specifically, for electrons with spin σ , these topological edge states will possess two energies,

$$E_\sigma = \pm \frac{i[(i\mu - \gamma)t_{2L}t_{2R} + (t_{1L}t_{2L} - t_{1R}t_{2R})\lambda_\sigma]}{\sqrt{t_{2L}t_{2R}(4\lambda^2 + t_{2L}t_{2R})}}, \quad (5)$$

which are exact in the thermodynamic limit $N \rightarrow \infty$. When inserting them back into Eq. (4), one obtains four β values,

$$\beta_1^\sigma = -\frac{\alpha - K - A_+}{2}, \quad \beta_2^\sigma = -\frac{\alpha - K + A_+}{2}, \quad (6)$$

$$\beta_3^\sigma = -\frac{\alpha + K - A_-}{2}, \quad \beta_4^\sigma = -\frac{\alpha + K + A_-}{2}, \quad (7)$$

where $\alpha = [2(i\mu - \gamma)\lambda_\sigma - t_{1L}t_{2L}]/(2\lambda^2)$, $K = [t_{1L}t_{2L} + t_{1R}t_{2R} - \alpha t_{2L}t_{2R}]/\sqrt{t_{2L}t_{2R}(4\lambda^2 + t_{2L}t_{2R})}$, and $A_\pm = [3\alpha^2 - 2\epsilon - K^2 \pm 2(\epsilon\alpha - \alpha^3 - \kappa)/K]^{1/2}$, with $\kappa = -[2(i\mu - \gamma)\lambda_\sigma + t_{1R}t_{2R}]/\lambda^2$, $\epsilon = 4S_\sigma - 4P - 2 - t_{2L}t_{2R}/\lambda^2$, and

$$P = \frac{(t_{1L}t_{2L} + t_{1R}t_{2R})^2}{16\lambda^2 t_{2L}t_{2R}}, \quad (8)$$

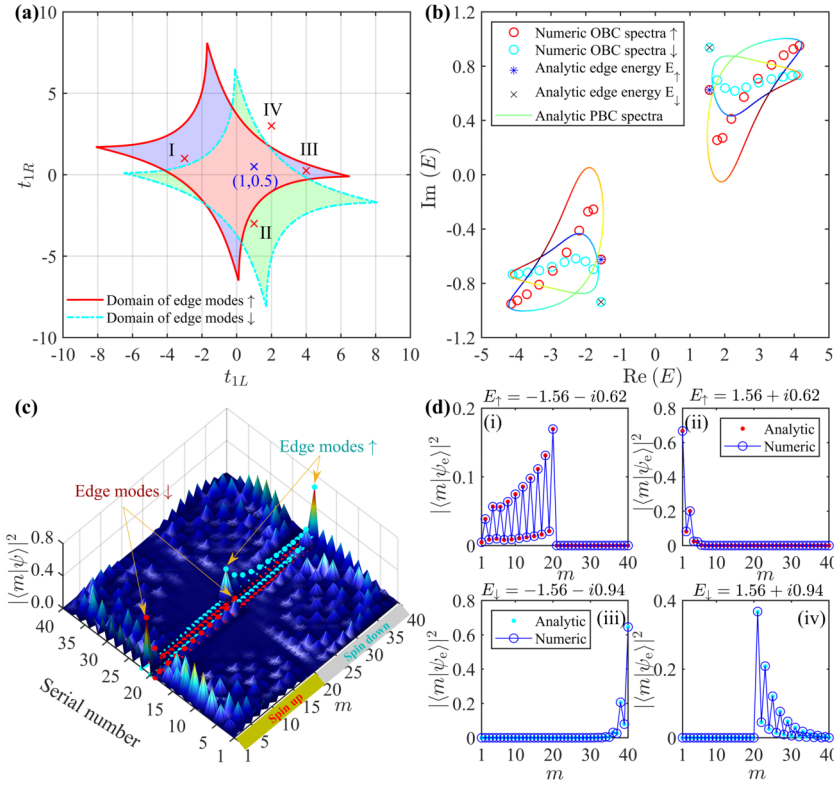


FIG. 2. (a) Phase diagram for topological edge modes with different spins, for given parameters $\gamma = 1$, $\mu = 2$, $\lambda = 4/5$, and $t_{2L} = t_{2R} = 2$. (b)–(d) show the OBC energy spectra, the 3D surface plot of eigenstates, and the analytic and numeric edge state profiles, respectively, obtained with $t_{1L} = 1$, $t_{1R} = 1/2$, and $N = 10$, corresponding to the blue cross in the overlapped pink region in (a). In (b), the colored directional curves denote the PBC spectra, while the blue asterisks and black crosses indicate the analytic spin-up edge energies E_{\uparrow} and the spin-down ones E_{\downarrow} , respectively. The other four parameter points denoted by red crosses in (a) will be shown in Fig. 3.

$$S_{\sigma} = \frac{[4\lambda_{\sigma}(i\mu - \gamma) - t_{1L}t_{2L} + t_{1R}t_{2R}]^2}{16\lambda^2(4\lambda^2 + t_{2L}t_{2R})}. \quad (9)$$

In terms of these four β values associated to E_{σ} , the eigenfunctions of topological edge states in the thermodynamic limit can be explicitly expressed as $|\psi_e\rangle = \sum_{m=1}^{4N} \psi_m |m\rangle = (\psi_{1A}^{\uparrow}, \psi_{1B}^{\uparrow}, \dots, \psi_{NA}^{\uparrow}, \psi_{NB}^{\uparrow}, \psi_{1A}^{\downarrow}, \psi_{1B}^{\downarrow}, \dots, \psi_{NA}^{\downarrow}, \psi_{NB}^{\downarrow})^T$. To be specific, for electronic states with spin up (i.e., $\sigma = \uparrow$), the state components read

$$\begin{aligned} \psi_{nA}^{\uparrow} &= \sum_{j=1}^4 c_j \phi(\beta_j^{\uparrow}) \beta_j^{\uparrow n}, & \psi_{nB}^{\uparrow} &= \sum_{j=1}^4 c_j \beta_j^{\uparrow n}, \\ \psi_{nA}^{\downarrow} &= \psi_{nB}^{\downarrow} = 0, \end{aligned} \quad (10)$$

otherwise, for spin-down electronic states ($\sigma = \downarrow$), these state components should take the form

$$\begin{aligned} \psi_{nA}^{\uparrow} &= \psi_{nB}^{\uparrow} = 0, & \psi_{nA}^{\downarrow} &= \sum_{j=1}^4 c_j \phi(\beta_j^{\downarrow}) \beta_j^{\downarrow n}, \\ \psi_{nB}^{\downarrow} &= \sum_{j=1}^4 c_j \beta_j^{\downarrow n}, \end{aligned} \quad (11)$$

where

$$\phi(\beta_j^{\sigma}) = \frac{R_+(\beta_j^{\sigma})}{E_{\sigma} - G(\lambda_{\sigma}, \beta_j^{\sigma})}, \quad (12)$$

and c_j are size-dependent complex coefficients given by

$$c_1 = g(\phi_{34}\beta_2^{\sigma N+1} + \phi_{42}\beta_3^{\sigma N+1} + \phi_{23}\beta_4^{\sigma N+1}), \quad (13)$$

$$c_2 = g(\phi_{43}\beta_1^{\sigma N+1} + \phi_{14}\beta_3^{\sigma N+1} + \phi_{31}\beta_4^{\sigma N+1}), \quad (14)$$

$$c_3 = g(\phi_{24}\beta_1^{\sigma N+1} + \phi_{41}\beta_2^{\sigma N+1} + \phi_{12}\beta_4^{\sigma N+1}), \quad (15)$$

$$c_4 = g(\phi_{32}\beta_1^{\sigma N+1} + \phi_{13}\beta_2^{\sigma N+1} + \phi_{21}\beta_3^{\sigma N+1}), \quad (16)$$

with $\phi_{ij} = \phi(\beta_i^{\sigma}) - \phi(\beta_j^{\sigma})$ and g being a free constant used to normalize the eigenvector $|\psi_e\rangle$ such that $\langle \psi_e | \psi_e \rangle = 1$. Note here that, for clarity, we have arranged the former $2N$ components in $|\psi_e\rangle$ to host electrons with spin up, while allocating the latter $2N$ ones for electrons with spin down. As can be verified, these topological edge states with eigenenergies E_{σ} are available only when the inequality

$$|-P + S_{\sigma} \pm \sqrt{(-P + S_{\sigma} + 1)^2 + 4P}| \leq \left| 1 + \frac{t_{2L}t_{2R}}{2\lambda^2} \right| \quad (17)$$

is satisfied, where P and S_{σ} are given by Eqs. (8) and (9).

We emphasize that the closed-form solutions (5), (10), and (11) for topological edge states with spin σ are asymptotically exact in the thermodynamic limit, but, however, are also accurate enough for finite lattice size $N \geq 5$, with errors generally below 1%. So is the parameter condition (17), which defines the domains of topological edge states with different spins. For illustration, we demonstrate in Fig. 2 four topological edge states allowed in an antichiral zigzag lattice with $N = 10$, for a typical set of system parameters specified by the blue cross in the overlapped pink region of the phase diagram in Fig. 2(a), which results from Eq. (17) for both spins. It is clearly seen that these four edge modes, two for spin up and two for spin down, as denoted by the red and cyan solid circles in Fig. 2(c), respectively, exhibit excellent consistency with numerical calculations based on Hamiltonian (1) [see Figs. 2(b) and 2(d)]. Further, in Fig. 2(d), one can find that the two topological edge modes associated with two E_{\uparrow} (or

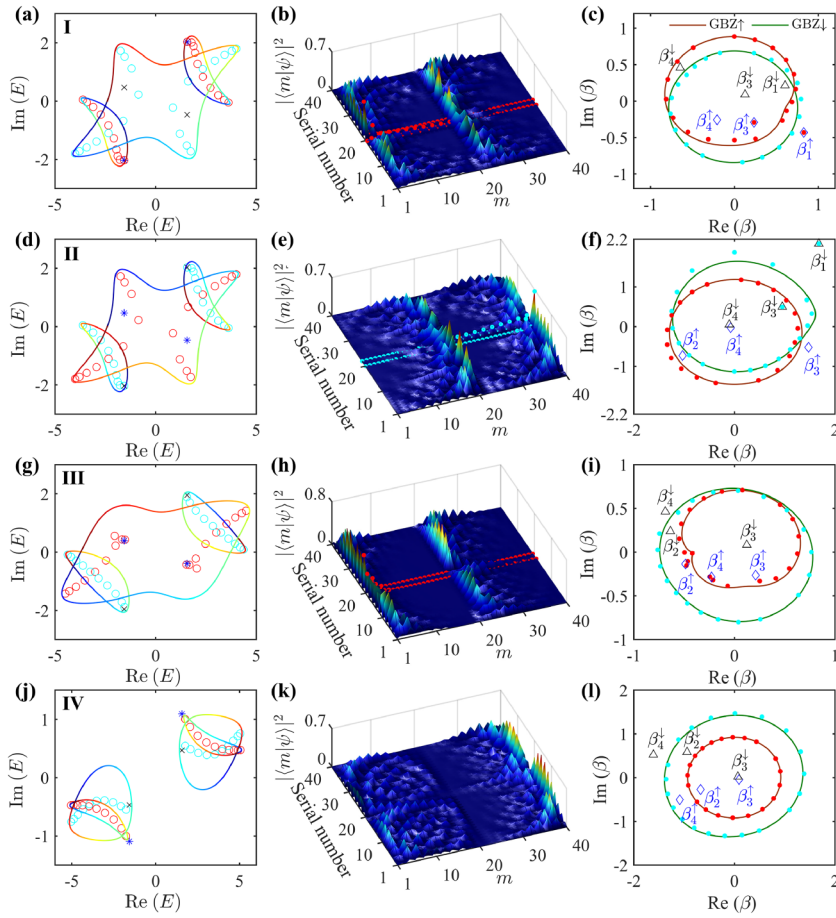


FIG. 3. Dual BBC for predicting topological edge states with different spins. The energy spectra (left), 3D surface plot of eigenstates (middle), and the GBZ \uparrow and GBZ \downarrow contours along with four β_j^\uparrow points (blue diamonds) and four β_j^\downarrow points (black triangles) (right). We use $t_{1L} = -3, t_{1R} = 1$ for case I, $t_{1L} = 1, t_{1R} = -3$ for case II, $t_{1L} = 4, t_{1R} = 1/4$ for case III, and $t_{1L} = 2, t_{1R} = 3$ for case IV, corresponding to parameter points I–IV in Fig. 2(a).

two E_\downarrow) have distinctly different intensity profiles, indicating that no exceptional points take place therein. This is a natural consequence of the non-Hermitian Hamiltonian that respects SLS † , by which its eigenenergies come in $(E, -E)$ pairs.

An inspection of these analytic solutions reveals that, in the presence of the SO coupling (i.e., $\lambda \neq 0$), the topological edge states generally possess four energy points in the complex plane, each of which could be separated from the energy continuum of the bulk when N approaches infinity, as seen in Fig. 2(b). Only when the parameter relation $t_{1L}t_{2L} = t_{1R}t_{2R}$ is met do the spin-up and spin-down edge energies coincide (i.e., spectral degeneracy). We term these analytic solutions topological edge states, not only because they exhibit non-trivial localization on the boundaries [see Fig. 2(c)] and a clear separation in energy spectrum from the bulk states [see Fig. 2(b)], but also because they have a genuine topological origin.

As a matter of fact, for predicting the existence of spin-up and spin-down topological edge states, we can define two topological winding numbers W_\uparrow and W_\downarrow ,

$$W_\uparrow = \oint_{\text{GBZ}\uparrow} \frac{d\beta}{4\pi i} \text{tr} \left(\sigma_z Q^{-1}(\lambda) \frac{dQ(\lambda)}{d\beta} \right), \quad (18)$$

$$W_\downarrow = \oint_{\text{GBZ}\downarrow} \frac{d\beta}{4\pi i} \text{tr} \left(\sigma_z Q^{-1}(-\lambda) \frac{dQ(-\lambda)}{d\beta} \right), \quad (19)$$

expressed, respectively, as a complex integration of rational functions of β along the GBZ \uparrow or GBZ \downarrow contour, where Q is

a λ -dependent specific non-Hermitian matrix:

$$Q(\lambda) = \frac{\lambda}{4\beta} \begin{bmatrix} 0 & (2\beta + \alpha - K)^2 - A_+^2 \\ (2\beta + \alpha + K)^2 - A_-^2 & 0 \end{bmatrix}. \quad (20)$$

We emphasize that this Q quantity results from a factorization of $\det[\mathcal{H}_\uparrow(\lambda, \beta) - E_\uparrow]$ and represents a significant generalization of the one developed for zero modes in bipartite lattice models [33,69,82]. According to the general residue theorem [83], the above complex contour integration equates to that it counts whether certain values of β associated with edge modes lie inside or outside of the GBZ. Specifically, one can find W_\uparrow and W_\downarrow through two steps: First, determine the GBZ \uparrow and GBZ \downarrow of the bulk states, which can be done either numerically or analytically [73]; second, calculate the four β_j^σ values using Eqs. (6) and (7) for given E_σ . Then, $W_\sigma = 1$ if only β_3^σ and β_4^σ lie inside of the GBZ σ contour. Otherwise, $W_\sigma = 0$. Only when the topological invariants are nonzero do the topological edge states exist, which is the so-called non-Hermitian BBC. As the system has two topological invariants (18) and (19) that work independently for predicting the topological edge states, we would like to term such a BBC as a dual BBC. Remarkably, letting $|\beta_{1,2}^\sigma| = |\beta_{3,4}^\sigma|$, one can exactly reproduce what the existence condition (17) shows for topological edge states (see Supplemental Fig. 3 in Ref. [73]).

To show this dual BBC, we consider the four parameter points denoted by I–IV (red crosses) in Fig. 2(a). We first demonstrate the energy spectra and eigenstates caused by these parameters in Fig. 3. It is obvious that, while cases

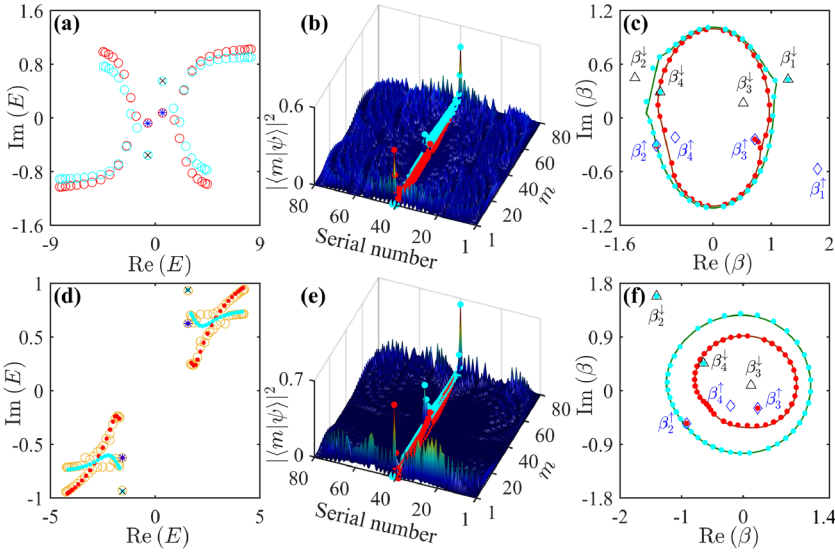


FIG. 4. Demonstration of dual BBC for either (a)–(c) the proposed Hamiltonian (1) that involves a larger SO coupling ($\lambda = 3$), or (d)–(f) the Hamiltonian (1) added by an off-diagonal perturbation \hat{H}_{per} , keeping other parameters the same as in Fig. 2. In (d), the bulk energy spectra in the absence of \hat{H}_{per} , denoted by red (spin-up) and cyan (spin-down) dots, are also plotted. In (f), the GBZ contours are calculated from the unperturbed Hamiltonian (1).

I and III admit topological spin-up edge states only, there exist spin-down edge states in case II and no topological edge states in case IV, as exactly predicted by the phase diagram in Fig. 2(a). Moreover, once the parameter points locate within the domain, our analytic solutions for either the spin-up or the spin-down edge states exhibit a striking agreement with the numerical results, even though only ten cells are calculated [see the red solid circles in Figs. 3(b) and 3(h) and the cyan solid circles in Fig. 3(e)]. Then, we calculate the GBZ \uparrow and GBZ \downarrow either numerically at $N = 10$ or analytically at $N = \infty$, which are traced by the middle two roots of Eq. (4) [33]. The results are shown in the rightmost column and, meanwhile, four β_j^\uparrow values (blue diamonds) for spin-up edge states and four β_j^\downarrow values (black triangles) for spin-down ones are provided therein (some large β_j^σ values are not shown). One can find easily that for case I, $W_\uparrow = 1$ and $W_\downarrow = 0$, for case II, $W_\uparrow = 0$ and $W_\downarrow = 1$, for case III, $W_\uparrow = 1$ and $W_\downarrow = 0$, and for case IV, $W_\uparrow = 0$ and $W_\downarrow = 0$, once again agreeing well with the numerical results shown in the middle column, hence confirming our conjecture of dual BBC.

One may wonder whether such dual BBC remains when a strong SLS † -symmetric coupling is added. To clear up this concern, we consider two different yet SLS † -symmetric Hamiltonians; one is the proposed Hamiltonian (1) yet involving a larger SO coupling value $\lambda = 3$, and the other is equal to the Hamiltonian (1) plus an off-diagonal perturbed term $\hat{H}_{\text{per}} = \lambda_p \sum_{n=1}^N (\hat{a}_n^\dagger \sigma_x \hat{b}_n - \hat{b}_n^\dagger \sigma_x \hat{a}_n) + \lambda_p^* \sum_{n=1}^{N-1} (-\hat{a}_{n+1}^\dagger \sigma_x \hat{b}_n + \hat{b}_n^\dagger \sigma_x \hat{a}_{n+1})$, where $\lambda_p = i/10 - \sqrt{3}/10$. The results are provided with Fig. 4, using a zigzag lattice of $N = 20$ cells. One can clearly see that our analytical solutions for topological edge states are in perfect agreement with their numerical solutions, and can be predicted by the topological invariants calculated by counting $\beta_{3,4}^\sigma$ within GBZ contours, whether the model used is the Hamiltonian (1) that has exact asymptotic solutions [see Figs. 4(a)–4(c)] or the perturbed one that does not admit exact solutions [see Figs. 4(d)–4(f)]. Particularly, in the latter case, it is exhibited that the bulk

states have been significantly altered by perturbation, whereas the topological edge states remain almost unchanged.

We finally point out that, in the presence of SO coupling, such topological edge states can admit zero energy $E_\sigma = 0$, if the parameter conditions $\mu = 0$ and $\gamma = (t_{1L}t_{2L} - t_{1R}t_{2R})\lambda_\sigma / (t_{2L}t_{2R})$ are met simultaneously. When $t_{1L}t_{2L} = t_{1R}t_{2R}$ is further satisfied, the Kramers degeneracy $E_\uparrow = E_\downarrow = 0$ can be attained. It is worth noting that, when $\mu = 0$, the Hamiltonian (1) will respect the time-reversal symmetry, by which its eigenenergies come in (E, E^*) pairs [47]. We demonstrate in Figs. 5(a) and 5(b) the degenerate zero modes for spin-up edge states occurring with a ten-cell zigzag lattice and in Figs. 5(c) and 5(d) their strong immunity to disorder when the lattice potential μ of the fifth cell is changed from zero to one, i.e., letting $\mu = 1$ at $n = 5$ (the other parameters are kept unchanged). This is not surprising because these edge modes are protected by the topology and the SLS † of the RM system and thus can survive until the phase transitions take place.

In conclusion, within the 1D non-Hermitian RM model, we unveiled a previously overlooked yet significant symmetry, alias SLS † , which is also relevant to the topology of non-Hermitian systems, including those with broken CS. We then established a dual BBC for interacting spinful electrons, by which one can realize a robust dual topological insulator phase in an SO-coupled zigzag lattice [84], or in a nonequilibrium setting assisted by the Floquet band engineering technique [85]. Moreover, our theory has enabled the study of topological edge states without a topological analysis of the bulk band structure, which is particularly helpful on the experimental side. Taking into consideration that the SO coupling is the cornerstone of the topological physics across a wide variety of materials with broken inversion symmetry [86], this dual BBC principle, which has an in-built SO feature, may also offer a fresh perspective for testing some SO-related physics such as spin-charge separation [87] and spin current generation [88].

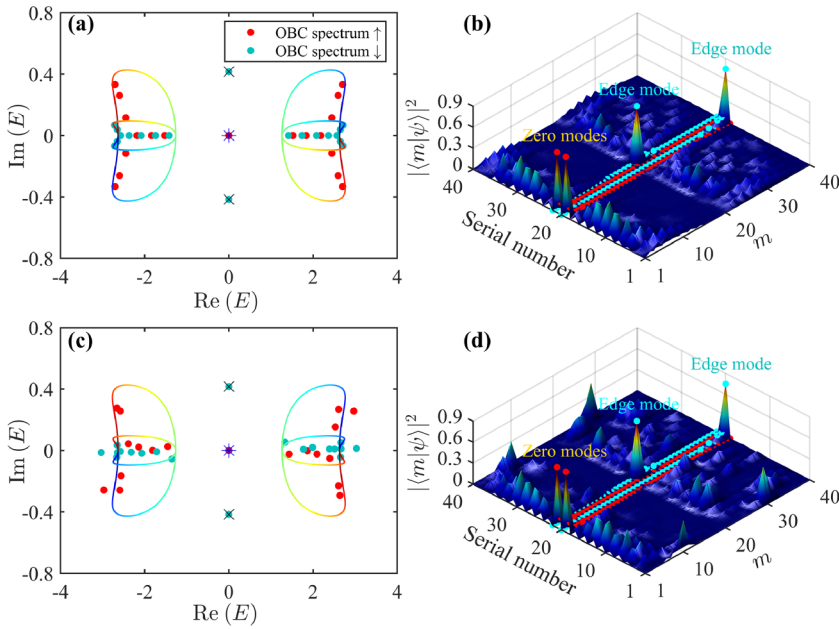


FIG. 5. (a), (b) Topological zero modes occurring in a ten-cell zigzag lattice, with $\mu = 0$, $\gamma = 4/15$, $\lambda = 4/5$, $t_{1L} = 1$, $t_{1R} = 1/3$, and $t_{2L} = t_{2R} = 2$, and (c), (d) their robustness against disorder, by changing the lattice potential μ of the fifth cell from 0 to 1.

This work was supported by the National Natural Science Foundation of China (Grants No. 12374301, No. 11974075, and No. 12122407) and the National Key Research and Development Program of China (Grant No. 2021YFA1200700). L.Y. thanks the sponsorship from Yangyang Development Fund.

- [1] A. Bansil, H. Lin, and T. Das, *Colloquium: Topological band theory*, *Rev. Mod. Phys.* **88**, 021004 (2016).
- [2] T. Ozawa, H. M. Price, A. Amo, N. Goldman, M. Hafezi, L. Lu, M. C. Rechtsman, D. Schuster, J. Simon, O. Zilberberg, and I. Carusotto, Topological photonics, *Rev. Mod. Phys.* **91**, 015006 (2019).
- [3] B. Xie, H. X. Wang, X. Zhang, P. Zhan, J. H. Jiang, M. Lu, and Y. Chen, Higher-order band topology, *Nat. Rev. Phys.* **3**, 520 (2021).
- [4] J. C. Y. Teo and C. L. Kane, Topological defects and gapless modes in insulators and superconductors, *Phys. Rev. B* **82**, 115120 (2010).
- [5] P. Delplace, D. Ullmo, and G. Montambaux, Zak phase and the existence of edge states in graphene, *Phys. Rev. B* **84**, 195452 (2011).
- [6] R. Süsstrunk and S. D. Huber, Classification of topological phonons in linear mechanical metamaterials, *Proc. Natl. Acad. Sci. USA* **113**, E4767 (2016).
- [7] K. Yatsugi, T. Yoshida, T. Mizoguchi, Y. Kuno, H. Iizuka, Y. Tadokoro, and Y. Hatsugai, Observation of bulk-edge correspondence in topological pumping based on a tunable electric circuit, *Commun. Phys.* **5**, 180 (2022).
- [8] H. Xue, Y. Yang, and B. Zhang, Topological acoustics, *Nat. Rev. Mater.* **7**, 974 (2022).
- [9] Y. Fu and H. Qin, Topological phases and bulk-edge correspondence of magnetized cold plasmas, *Nat. Commun.* **12**, 3924 (2021).
- [10] L. Lu, J. D. Joannopoulos, and M. Soljačić, Topological photonics, *Nat. Photonics* **8**, 821 (2014).
- [11] S. Mittal, S. Ganeshan, J. Fan, A. Vaezi, and M. Hafezi, Measurement of topological invariants in a 2D photonic system, *Nat. Photonics* **10**, 180 (2016).
- [12] Z. Wang, Y. Chong, J. D. Joannopoulos, and M. Soljačić, Observation of unidirectional backscattering-immune topological electromagnetic states, *Nature (London)* **461**, 772 (2009).
- [13] C. K. Chiu, J. C. Y. Teo, A. P. Schnyder, and S. Ryu, Classification of topological quantum matter with symmetries, *Rev. Mod. Phys.* **88**, 035005 (2016).
- [14] X. L. Qi and S. C. Zhang, Topological insulators and superconductors, *Rev. Mod. Phys.* **83**, 1057 (2011).
- [15] T. O. Wehling, A. M. Black-Schaffer, and A. V. Balatsky, Dirac materials, *Adv. Phys.* **63**, 1 (2014).
- [16] S. Chen, L. Bu, C. Pan, C. Hou, F. Baronio, P. Grelu, and N. Akhmediev, Modulation instability-rogue wave correspondence hidden in integrable systems, *Commun. Phys.* **5**, 297 (2022).
- [17] Y. Ashida, Z. Gong, and M. Ueda, Non-Hermitian physics, *Adv. Phys.* **69**, 249 (2020).
- [18] Z. Gong, Y. Ashida, K. Kawabata, K. Takasan, S. Higashikawa, and M. Ueda, Topological phases of non-Hermitian systems, *Phys. Rev. X* **8**, 031079 (2018).
- [19] R. El-Ganainy, K. G. Makris, M. Khajavikhan, Z. H. Musslimani, S. Rotter, and D. N. Christodoulides, Non-Hermitian physics and PT symmetry, *Nat. Phys.* **14**, 11 (2018).
- [20] H. Shen, B. Zhen, and L. Fu, Topological band theory for non-Hermitian Hamiltonians, *Phys. Rev. Lett.* **120**, 146402 (2018).
- [21] C. Coulais, R. Fleury, and J. van Wezel, Topology and broken Hermiticity, *Nat. Phys.* **17**, 9 (2021).
- [22] S. Yao and Z. Wang, Edge states and topological invariants of non-Hermitian systems, *Phys. Rev. Lett.* **121**, 086803 (2018).
- [23] F. Song, S. Yao, and Z. Wang, Non-Hermitian skin effect and chiral damping in open quantum systems, *Phys. Rev. Lett.* **123**, 170401 (2019).
- [24] S. Longhi, Probing non-Hermitian skin effect and non-Bloch phase transitions, *Phys. Rev. Res.* **1**, 023013 (2019).

- [25] C. H. Lee and R. Thomale, Anatomy of skin modes and topology in non-Hermitian systems, *Phys. Rev. B* **99**, 201103(R) (2019).
- [26] N. Okuma, K. Kawabata, K. Shiozaki, and M. Sato, Topological origin of non-Hermitian skin effects, *Phys. Rev. Lett.* **124**, 086801 (2020).
- [27] K. Zhang, Z. Yang, and C. Fang, Correspondence between winding numbers and skin modes in non-Hermitian systems, *Phys. Rev. Lett.* **125**, 126402 (2020).
- [28] T. E. Lee, Anomalous edge state in a non-Hermitian lattice, *Phys. Rev. Lett.* **116**, 133903 (2016).
- [29] Y. Xiong, Why does bulk boundary correspondence fail in some non-Hermitian topological models, *J. Phys. Commun.* **2**, 035043 (2018).
- [30] F. K. Kunst, E. Edvardsson, J. C. Budich, and E. J. Bergholtz, Biorthogonal bulk-boundary correspondence in non-Hermitian systems, *Phys. Rev. Lett.* **121**, 026808 (2018).
- [31] E. Edvardsson, F. K. Kunst, T. Yoshida, and E. J. Bergholtz, Phase transitions and generalized biorthogonal polarization in non-Hermitian systems, *Phys. Rev. Res.* **2**, 043046 (2020).
- [32] S. Yao, F. Song, and Z. Wang, Non-Hermitian Chern bands, *Phys. Rev. Lett.* **121**, 136802 (2018).
- [33] K. Yokomizo and S. Murakami, Non-Bloch band theory of non-Hermitian systems, *Phys. Rev. Lett.* **123**, 066404 (2019).
- [34] Z. Yang, K. Zhang, C. Fang, and J. Hu, Non-Hermitian bulk-boundary correspondence and auxiliary generalized Brillouin zone theory, *Phys. Rev. Lett.* **125**, 226402 (2020).
- [35] X. Zhu, H. Wang, S. K. Gupta, H. Zhang, B. Xie, M. Lu, and Y. Chen, Photonic non-Hermitian skin effect and non-Bloch bulk-boundary correspondence, *Phys. Rev. Res.* **2**, 013280 (2020).
- [36] H. G. Zirnstein, G. Refael, and B. Rosenow, Bulk-boundary correspondence for non-Hermitian Hamiltonians via Green functions, *Phys. Rev. Lett.* **126**, 216407 (2021).
- [37] C. Hou, L. Li, S. Chen, Y. Liu, L. Yuan, Y. Zhang, and Z. Ni, Deterministic bulk-boundary correspondences for skin and edge modes in a general two-band non-Hermitian system, *Phys. Rev. Res.* **4**, 043222 (2022).
- [38] C. Hou, L. Li, G. Wu, Y. Ruan, S. Chen, and F. Baronio, Topological edge states in one-dimensional non-Hermitian Su-Schrieffer-Heeger systems of finite lattice size: Analytical solutions and exceptional points, *Phys. Rev. B* **108**, 085425 (2023).
- [39] T. Helbig, T. Hofmann, S. Imhof, M. Abdelghany, T. Kiessling, L. W. Molenkamp, C. H. Lee, A. Szameit, M. Greiter, and R. Thomale, Generalized bulk-boundary correspondence in non-Hermitian topoelectrical circuits, *Nat. Phys.* **16**, 747 (2020).
- [40] A. Ghatak, M. Brandenbourger, J. van Wezel, and C. Coullais, Observation of non-Hermitian topology and its bulk-edge correspondence in an active mechanical metamaterial, *Proc. Natl. Acad. Sci. USA* **117**, 29561 (2020).
- [41] S. Weidemann, M. Kremer, T. Helbig, T. Hofmann, A. Stegmaier, M. Greiter, R. Thomale, and A. Szameit, Topological funneling of light, *Science* **368**, 311 (2020).
- [42] R. Ye, Y. He, G. Li, L. Wang, X. Wu, X. Qiao, Y. Zheng, L. Jin, D. W. Wang, L. Yuan, and X. Chen, Observation of non-Hermitian antichiral edge currents, [arXiv:2305.17853](https://arxiv.org/abs/2305.17853).
- [43] L. Xiao, T. Deng, K. Wang, G. Zhu, Z. Wang, W. Yi, and P. Xue, Non-Hermitian bulk-boundary correspondence in quantum dynamics, *Nat. Phys.* **16**, 761 (2020).
- [44] H. C. Po, A. Vishwanath, and H. Watanabe, Symmetry-based indicators of band topology in the 230 space groups, *Nat. Commun.* **8**, 50 (2017).
- [45] Z. Wang, X. Wang, Z. Hu, D. Bongiovanni, D. Jukić, L. Tang, D. Song, R. Morandotti, Z. Chen, and H. Buljan, Sub-symmetry-protected topological states, *Nat. Phys.* **19**, 992 (2023).
- [46] S. Ryu, A. P. Schnyder, A. Furusaki, and A. W. W. Ludwig, Topological insulators and superconductors: Tenfold way and dimensional hierarchy, *New J. Phys.* **12**, 065010 (2010).
- [47] K. Kawabata, K. Shiozaki, M. Ueda, and M. Sato, Symmetry and topology in non-Hermitian physics, *Phys. Rev. X* **9**, 041015 (2019).
- [48] M. J. Rice and E. J. Mele, Elementary excitations of a linearly conjugated diatomic polymer, *Phys. Rev. Lett.* **49**, 1455 (1982).
- [49] K. Takata and M. Notomi, Photonic topological insulating phase induced solely by gain and loss, *Phys. Rev. Lett.* **121**, 213902 (2018).
- [50] H. Zhao, X. Qiao, T. Wu, B. Midya, S. Longhi, and L. Feng, Non-Hermitian topological light steering, *Science* **365**, 1163 (2019).
- [51] Ş. K. Özdemir, S. Rotter, F. Nori, and L. Yang, Parity-time symmetry and exceptional points in photonics, *Nat. Mater.* **18**, 783 (2019).
- [52] Y. Yi and Z. Yang, Non-Hermitian skin modes induced by on-site dissipations and chiral tunneling effect, *Phys. Rev. Lett.* **125**, 186802 (2020).
- [53] C. H. Lee, L. Li, and J. Gong, Hybrid higher-order skin-topological modes in nonreciprocal systems, *Phys. Rev. Lett.* **123**, 016805 (2019).
- [54] C. L. Kane and E. J. Mele, Z_2 topological order and the quantum spin Hall effect, *Phys. Rev. Lett.* **95**, 146802 (2005).
- [55] C. L. Kane and E. J. Mele, Quantum spin Hall effect in graphene, *Phys. Rev. Lett.* **95**, 226801 (2005).
- [56] B. A. Bernevig, T. L. Hughes, and S. C. Zhang, Quantum spin Hall effect and topological phase transition in HgTe quantum wells, *Science* **314**, 1757 (2006).
- [57] Z. Q. Jiao, S. Longhi, X. W. Wang, J. Gao, W. H. Zhou, Y. Wang, Y. X. Fu, L. Wang, R. J. Ren, L. F. Qiao, and X. M. Jin, Experimentally detecting quantized Zak phases without chiral symmetry in photonic lattices, *Phys. Rev. Lett.* **127**, 147401 (2021).
- [58] M. Eschbach, M. Lanius, C. Niu, E. Młyńczak, P. Gospodarič, J. Kellner, P. Schüffelgen, M. Gehlmann, S. Döring, E. Neumann, M. Luysberg, G. Mussler, L. Plucinski, M. Morgenstern, D. Grützmacher, G. Bihlmayer, S. Blügel, and C. M. Schneider, Bi_1Te_1 is a dual topological insulator, *Nat. Commun.* **8**, 14976 (2017).
- [59] H.-P. Xue, R. Sun, X. Yang, A. Comstock, Y. Liu, B. Ge, J.-N. Liu, Y.-S. Wei, Q.-L. Yang, X.-S. Gai, Z.-Z. Gong, Z.-K. Xie, N. Li, D. Sun, X.-Q. Zhang, W. He, and Z.-H. Cheng, Dual topology of dirac electron transport and photogalvanic effect in low-dimensional topological insulator superlattices, *Adv. Mater.* **35**, 2208343 (2023).
- [60] A. Anirban, Dual topological insulator found in superlattice, *Nat. Rev. Phys.* **5**, 270 (2023).
- [61] J. M. Zeuner, M. C. Rechtsman, Y. Plotnik, Y. Lumer, S. Nolte, M. S. Rudner, M. Segev, and A. Szameit, Observation of a

- topological transition in the bulk of a non-Hermitian system, *Phys. Rev. Lett.* **115**, 040402 (2015).
- [62] S. Longhi, Topological phase transition in non-Hermitian quasicrystals, *Phys. Rev. Lett.* **122**, 237601 (2019).
- [63] E. J. Bergholtz, J. C. Budich, and F. K. Kunst, Exceptional topology of non-Hermitian systems, *Rev. Mod. Phys.* **93**, 015005 (2021).
- [64] Y. Zhang, Y. W. Tan, H. L. Stormer, and P. Kim, Experimental observation of the quantum Hall effect and Berry's phase in graphene, *Nature (London)* **438**, 201 (2005).
- [65] C. C. Liu, W. Feng, and Y. Yao, Quantum spin Hall effect in silicene and two-dimensional germanium, *Phys. Rev. Lett.* **107**, 076802 (2011).
- [66] Y. Liu, A. Dobrinsky, and B. I. Yakobson, Graphene edge from armchair to zigzag: The origins of nanotube chirality? *Phys. Rev. Lett.* **105**, 235502 (2010).
- [67] Y. Li, C. Liang, C. Wang, C. Lu, and Y. C. Liu, Gain-loss-induced hybrid skin-topological effect, *Phys. Rev. Lett.* **128**, 223903 (2022).
- [68] S. Xia, Y. Liang, L. Tang, D. Song, J. Xu, and Z. Chen, Photonic realization of a generic type of graphene edge states exhibiting topological flat band, *Phys. Rev. Lett.* **131**, 013804 (2023).
- [69] K. Esaki, M. Sato, K. Hasebe, and M. Kohmoto, Edge states and topological phases in non-Hermitian systems, *Phys. Rev. B* **84**, 205128 (2011).
- [70] A. Manchon, H. C. Koo, J. Nitta, S. M. Frolov, and R. A. Duine, New perspectives for Rashba spin-orbit coupling, *Nat. Mater.* **14**, 871 (2015).
- [71] H. Min, J. E. Hill, N. A. Sinitsyn, B. R. Sahu, L. Kleinman, and A. H. MacDonald, Intrinsic and Rashba spin-orbit interactions in graphene sheets, *Phys. Rev. B* **74**, 165310 (2006).
- [72] C. C. Liu, H. Jiang, and Y. Yao, Low-energy effective Hamiltonian involving spin-orbit coupling in silicene and two-dimensional germanium and tin, *Phys. Rev. B* **84**, 195430 (2011).
- [73] See Supplemental Material at <http://link.aps.org/supplemental/10.1103/PhysRevB.110.L041103> for details of solving the RM model in real space, the closed-form topological edge-mode solutions, the symmetry properties of the RM Hamiltonian, two topological invariants proposed for predicting topological edge modes, an approach to calculating the exact GBZ, the proofs of several typical symmetry types, the RM model with Rashba spin-orbit (SO) coupling being included, and the relevance of our proposed symmetry to the topological winding number, which includes Refs. [74–77].
- [74] S.-Q. Shen, *Topological Insulators: Dirac Equation in Condensed Matters* (Springer, Berlin, 2013).
- [75] A. W. W. Ludwig, Topological phases: Classification of topological insulators and superconductors of non-interacting fermions, and beyond, *Phys. Scr.* **T168**, 014001 (2016).
- [76] H. Xue, Q. Wang, B. Zhang, and Y. D. Chong, Non-Hermitian Dirac cones, *Phys. Rev. Lett.* **124**, 236403 (2020).
- [77] L. Fu and C. L. Kane, Topological insulators with inversion symmetry, *Phys. Rev. B* **76**, 045302 (2007).
- [78] X. Wu, L. Wang, S. Chen, X. Chen, and L. Yuan, Transition characteristics of non-Hermitian skin effects in a zigzag lattice without chiral symmetry, *Adv. Phys. Res.* **2**, 2300007 (2023).
- [79] Q. Wang and Y. D. Chong, Non-Hermitian photonic lattices: Tutorial, *J. Opt. Soc. Am. B* **40**, 1443 (2023).
- [80] S. Weimann, M. Kremer, Y. Plotnik, Y. Lumer, S. Nolte, K. G. Makris, M. Segev, M. C. Rechtsman, and A. Szameit, Topologically protected bound states in photonic parity-time-symmetric crystals, *Nat. Mater.* **16**, 433 (2017).
- [81] M. Parto, S. Wittek, H. Hodaei, G. Harari, M. A. Bandres, J. Ren, M. C. Rechtsman, M. Segev, D. N. Christodoulides, and M. Khajavikhan, Edge-mode lasing in 1D topological active arrays, *Phys. Rev. Lett.* **120**, 113901 (2018).
- [82] S.-D. Liang and G.-Y. Huang, Topological invariance and global Berry phase in non-Hermitian systems, *Phys. Rev. A* **87**, 012118 (2013).
- [83] T. Needham, *Visual Complex Analysis, 25th Anniversary Edition* (Oxford University Press, Oxford, UK, 2023).
- [84] S. Liu, H. Yin, D. J. Singh, and P. F. Liu, Ta₄SiTe₄: A possible one-dimensional topological insulator, *Phys. Rev. B* **105**, 195419 (2022).
- [85] M. S. Rudner and N. H. Lindner, Band structure engineering and non-equilibrium dynamics in Floquet topological insulators, *Nat. Rev. Phys.* **2**, 229 (2020).
- [86] V. Galitski and I. B. Spielman, Spin-orbit coupling in quantum gases, *Nature (London)* **494**, 49 (2013).
- [87] C. Kim, A. Y. Matsuura, Z. X. Shen, N. Motoyama, H. Eisaki, S. Uchida, T. Tohyama, and S. Maekawa, Observation of spin-charge separation in one-dimensional SrCuO₂, *Phys. Rev. Lett.* **77**, 4054 (1996).
- [88] W. Han, S. Maekawa, and X. C. Xie, Spin current as a probe of quantum materials, *Nat. Mater.* **19**, 139 (2020).